Geotechnical Aspects of Underground Construction in Soft Ground – Yoo, Park, Kim & Ban (Eds)

Stiffness reduction in soft Chicago clay during deep urban excavations

Young-Hoon Jung
Department of Civil Engineering, Kyung Hee University, Republic of Korea

Taesik Kim
Department of Civil Engineering, Hong Ik University, Republic of Korea

ABSTRACT: The nonlinearity and anisotropy are two key issues in evaluating the soil stiffness for the precise prediction of the displacement. Recent studies on the stress-strain behavior of Chicago clay, especially focused on the responses at small-strains, reveal the pattern of nonlinear stiffness degradation as the clay is stressed. Herein, we attempt to apply these observational responses of Chicago clay to an excavation problem. The finite element simulation of the excavation in the downtown Chicago area was conducted. At some observation locations, the simulations yield typical stress paths. Changes in nonlinearity and anisotropy were discussed by comparing computed and experimental stress paths. Even in the first few excavations, the reduction of shear stiffness could be significant in soft Chicago clay.

1 INTRODUCTION

The nonlinearity and anisotropy are two key issues in evaluating the soil stiffness for the precise prediction of the displacement. The evaluation of exact soil stiffness and thus soil deformation become crucial because of strict regulation in the displacement during construction even though the amount of displacement is sufficiently small to cause minor cosmetic problems. Increasing number of law suit tackling these issues demands high quality of prediction in soil deformation, and thus it requires the nonlinear and anisotropic characteristics of soils in urban excavation.

Recent studies on the stress-strain behavior of Chicago clay, especially focused on the responses at small-strains, reveal the pattern of nonlinear stiffness degradation as the clay is stressed. Herein, we attempt to apply these observational responses of Chicago clay to an excavation problem. The finite element simulation of the excavation in the downtown Chicago area was conducted. At some observation locations, the simulations yield typical stress paths. Changes in nonlinearity and anisotropy were discussed by comparing computed and experimental stress paths.

2 METHODOLOGY

The commercial program, PLAXIS (2010), were used to simulation the excavation. Figure 1 shows the finite element mesh. Slurry wall and slabs were modeled using beam-type elements. All the soils are modeled using triangular continuum element. Because of very low hydraulic conductivity of Chicago clay, the undrained condition is assumed in finite element analysis.

For characterizing Chicago clays, the constitutive model developed by Masin (2006) was employed. This model is based on the hypoplastic laws presented by Kolymbas (1991). Hypoplastic model obeys a single equation that defines the relation between stress and strain based on the direction of loading and other state varibles. This model incorporates an incremental form of the direction-dependent stiffnesses. To model the stiffness at large strains, it has a reference model with five parameters. Detailed plan view for the simulation is given in Figure 2.

Typical five Chicago clay layers–Blodgett, Deerfield, Park-Ridge, Tinley, and Valparios–and the fill on top surface were modeled with different constitutive model and material properties. Stratification properties and soil properties are summarized in Table 1.

The superficial fill materials were modeled using a modified Mohr-Coulomb model with pressure-dependent elastic Young's modulus given as

$$E = E^{ref}_{0} \left(\frac{p}{p^{ref}_{0}} \right)^{\alpha} \tag{1}$$

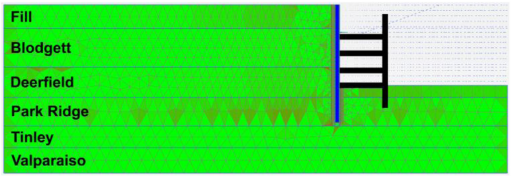

Figure 1. Finite element mesh for excavation.

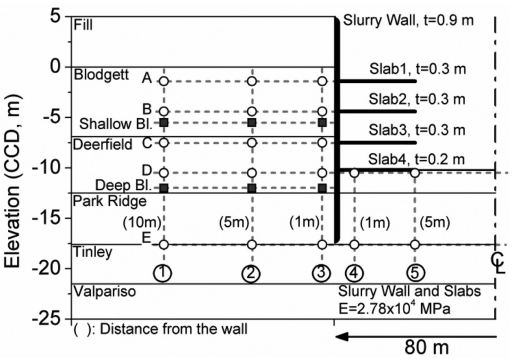

Figure 2. Detailed section view of the excavation site.

Table 1. Soil properties for soil layers.

Layer	EL (top) m	Unit Weight kN/m^3	OCR	K_0
Fill	6.0	17.28		0.43
Blodgett	−1.52	18.85	1.05	0.60
Deerfield (up)	−7.29	19.64	1.30	0.51
Deerfield (down)	−10.95	19.64	1.30	0.56
Park Ridge (up)	−14.60	19.64	4.76	1.06
Park Ridge (down)	−16.95	19.64	5.4	1.16
Tinley	−19.3	20.42	3.25	0.81

Table 2. Parameters for Mohr-Coulomb model with stress-dependent stiffness.

Parameter	Unit	Value	Description
E_0^{ref}	kPa	11610	Reference stiffness
p_0^{ref}	kPa	100	Reference stress
α	—	0.5	Stress dependence coefficient
ν	—	0.33	Primary loading Poisson's ratio
ϕ	deg.	30	Peak friction angle
c	kPa	10	Cohesion intercept
ψ	deg.	2	Dilatancy angle

where E_0^{ref} is the reference Young's modulus, p_0^{ref} is reference stress taken as 100 kPa, α is the exponent relating to stress-dependent nature of Young's modulus. Table 2 summarizes the model parameters for the modified Mohr-Coulomb model used in this study.

Four Chicago clay layers were modeled by the hypoplasticity model. The model parameters selected for each layer were summarized in Table 3.

Addition state-dependent parameters for describing evolution of the soil stiffness from small to large strains are listed in Table 4. Details on the selection of parameter values for Chicago clays were described in Sarabia (2012). The retaining wall consists of secant piles above the maximum excavation depth and tangent piles below. The bending stiffness above and below the maximum excavation depth were given different model parameters.

Table 3. Reference parameters for hypoplastic model.

Layer	ϕ'_{cv}	N	λ^*	κ^*	R
Blodgett	24.2	1.029	0.082	0.023	5×10^{-5}
Deerfield (up)	34.1	0.635	0.048	0.014	5×10^{-5}
Deerfield (down)	30.9	0.759	0.059	0.017	5×10^{-5}
Park Ridge (up)	33.4	0.660	0.050	0.014	5×10^{-5}
Park Ridge (down)	30.3	0.784	0.061	0.017	5×10^{-5}
Tinley	36.7	0.535	0.040	0.011	5×10^{-5}

Table 4. Hypoplasticity model parameters for evolution of the soil stiffness from small to large strains.

Parameter	Description
R	Maximum value of the norm of ||h||
m_R, m_T	Parameter relating the small-strain stiffness
β	Parameter accumulating intergranular strain
χ	Parameter for interpolating the stress state

The stiffness, EI, of the retaining wall are 3.33×10^6 and 1.571×10^6 kNm^2/m for the secant and tangent piles, respectively. Young's modulus for structural elements including slurry walls and slabs is 2.78×10^4 MPa. The staged construction of excavation and installation of slab are sequentially simulated with a number of numerical steps. A number of observation points were selected. As shown in Figure 2, a number of rows (from A to E) and columns (from ① to ⑤) are drawn. The observation point is selected in each intersection of a row and a column. The name of the observation point is designated by the name of the row and column used. For example, an observation point "B2" refers to the intersection of the row "B" and the column "2" in Figure 2.

3 RESULTS AND DISCUSSIONS

Figure 3 shows the stress paths at the selected observation points in Figure 2. The stresses were measured at five different stages. Initial stress points are indicated by "Initial" in figure 2. The stage denoted by "Slab 1" to "Slab 4" in figure 3 corresponds to the sequential excavation to corresponding depth marked in Figure 2. The observation points for figure 3a, i.e. A1 to E1, are located along the column 1 in Figure 2, 10-m away from the slurry wall horizontally.

Even though these observation points have different initial stresses due to their in-situ gravitational stress, the pattern in the stress paths are practically the same. The direction of the stress paths is approximately vertical for the first excavation of Slab 1, implying the increasing vertical stress while keeping constant pressure by reducing horizontal stress. Except for E1, the change in the stress path is immediate at the first excavation. The changes in the stress path appear minor at the following excavation stages. The stress path for E1 shows progressive increase in the deviator stress, q in the sequential excavations. Typical variation in q

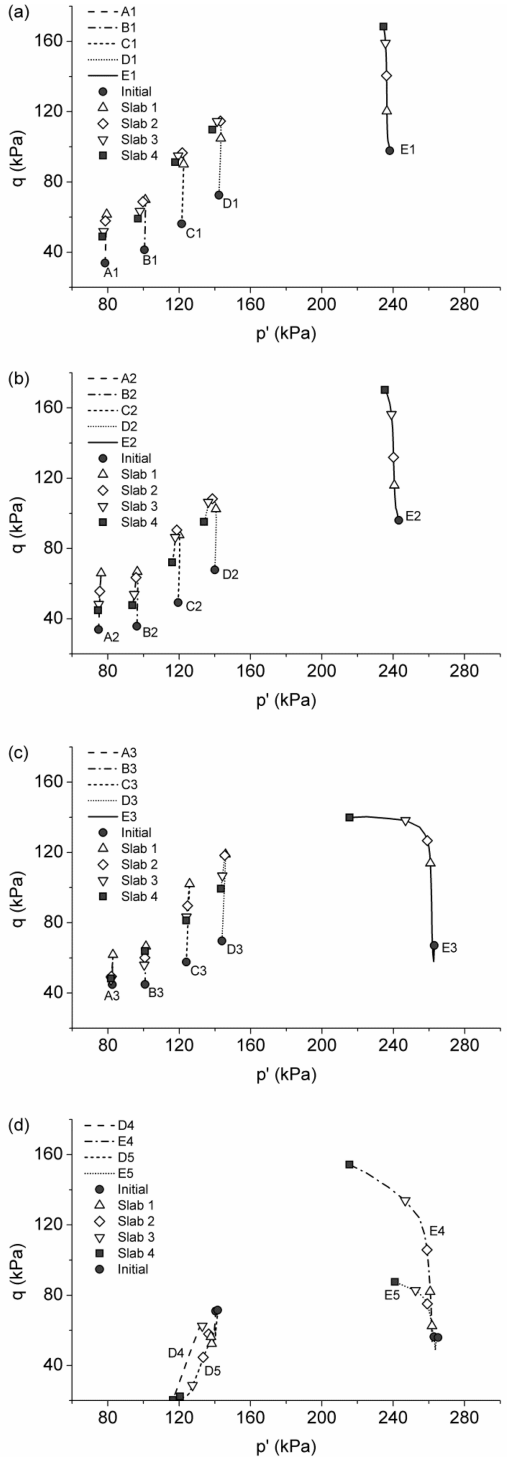

Figure 3. Stress paths for various observation points.

is approximately 20 kPa whereas the variation in E1 exceeds 60 kPa.

The variations of stresses for the second set of the observation points, A2 to E2, located 5-m away from

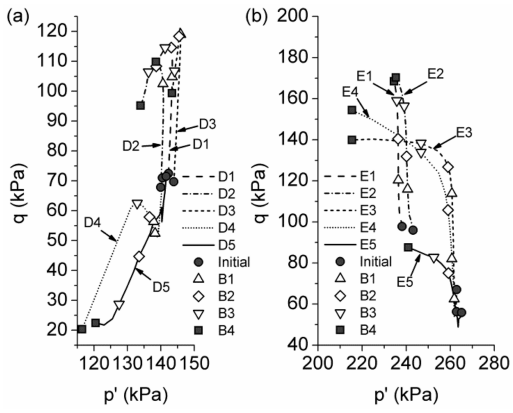

Figure 4. Stress paths for the observation points, D and E.

the slurry wall, are approximately the same as those for the first set of observation points, A1 to E1. Only slight difference exist where the final stress points for the second set move downward closer to their initial points than the first set. Nevertheless, the stress path for E2 is quite similar to the path for E1.

The third set of the observation points, A3 to E3, is located very closely to the slurry wall, only 1-m away from the wall. As shown in Figure 3(c), the stress paths for A3, B3, C3 and D3 are vertically straight as similarly as those for first and second set of the observation points, whereas the final stress points become closer clearly to the initial points than for the first and second sets. Significant change in the stress path direction can be found in the stress path for E3 located near the toe of the wall. For the first two stages, the stress path moves vertically but at the third excavation stage, "Slab 3", the pressure is reduced with the approximately constant deviator stress.

Figure 3(d) shows the variation of the stress paths for the observation points, D4, E4, D5, and E5. The paths for D4 and D5 both directing downward and right hand side are very close to the reduced extension path in the triaxial experiment. The paths for E4 and E5 both initially move vertically whereas the path for E5 cease to move earlier than the path for E4. The largest change in the stress path is found at the observation point, E4, showing the variation of approximately 100 kPa in the deviator stress.

Figure 5 shows the stress paths for the observation points located in the two depths where the block samples were taken. The samples were taken at a relatively shallow depth close to the row of B and a relatively deep depth close to the row of D in Fig. 2. As can be seen in Fig. 5, the stress paths for the shallow block virtually follow the same pattern such that the path moves vertically at the first excavation and subsequently moves downward with slight reduction of the pressure. From the initial value of q for the "shallow block" sample in Figure 5(a), the deviator stress, q, increases approximately by 30 kPa at the first excavation.

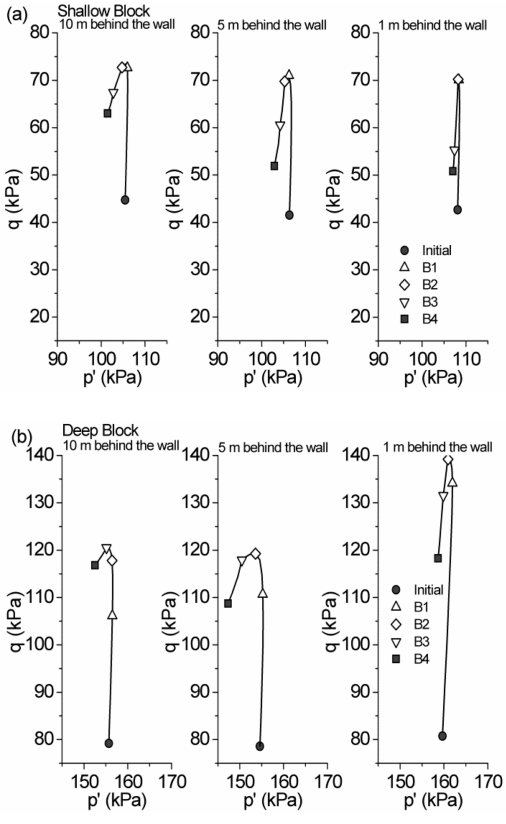

Figure 5. Stress paths for the points where block samples were taken.

Subsequent excavations result in the reduction of q with accompany by slight reduction of p' by about 5 kPa.

As shown in Figure 5(b), the stress paths for the deep block also vary similarly to those for the shallow block, except for the vertical movement of the stress path until third excavation. From its initial value, the deviator stress, q, increases in the first two excavation stages approximately by 40 kPa and more than 60 kPa in the location 1-m behind the wall. During remaining two excavations, the deviator stress and mean normal stress decrease as similarly as in the shallow block samples.

In summary, the major direction of the stress paths for the first and second excavation stages is vertical in p'-q space, which coincides with the compression with the constant mean normal stress (CPC) path in the triaixial test. Subsequent excavations result in the unloading paths of q with slight reduction of p', which is close to the triaxial extension path in the triaxial test. Numerical simulations predicts the magnitude of the increasing q for the first two excavations of 30 and 40 kPa in the shallow and deep block locations, respectively.

Figure 6 shows the stress-strain curves for two samples from "shallow block" and "deep block" locations. The stress path applied was the CPC (compression with

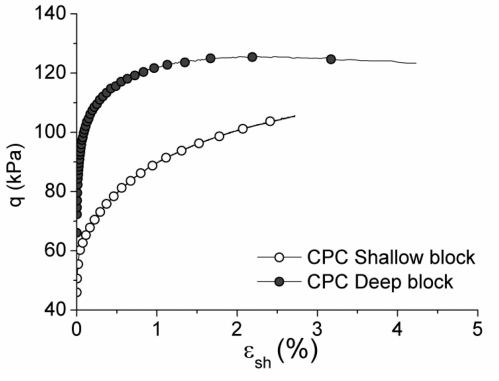

Figure 6. Shear stress-shear strain relationship in CPC path for shallow and deep block samples.

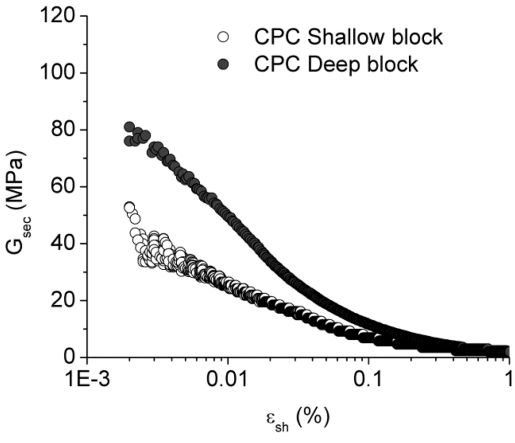

Figure 7. Degradation of shear stiffness in CPC path for shallow and deep block samples.

constant mean normal stress) path, which is close to the path observed in the finite element analyses shown in Figure 5.

Reminding that typical increase in the deviator stress during first two excavations are 30 and 40 kPa for two different blocks, the corresponding shear strains do not exceed 0.5%. Figure 7 shows the pattern of the shear stiffness degradation as a function of the shear strain. The reduction of the shear stiffness from its initial value is as much as 90% at the strain level of 0.5%. Therefore, significant change in shear stiffness, herein 90% reduction of shear stiffness, should be expected even in the first few stages of excavation in urban area.

4 CONCLUSIONS

The numerical study using finite element analyses was conducted to simulate staged excavation in the downtown area of Chicago. Within the commercial code of PLAXIS, hypoplasticity model was implemented to

model the small-strain nonlinear behavior of Chicago glacial tills. Typical five clay layers and the fill on the top surface were considered in the simulation. Retaining secant wall was modeled by the beam elements. Staged excavations and the installation of slabs were sequentially simulated. A number of observation points were located within the soil mass behind the wall. It was found that the majority of the stress paths observed at the different observation points are vertically straight in the first two excavations. These patterns of the stress paths are quite similar to those in the triaxial compression test with the constant mean normal stress. Subsequent excavations results in the unloading paths accompanying with decreasing deviator stress. Computed magnitude of the increasing deviator stress for the first two excavations is approximately 30 kPa at the depth where the shallow block samples were taken. The corresponding level of strains can also be estimated when investigating the stress-strain curve for the stress probe experiment of CPC. For the variation of the stress of 30 kPa in CPC test, the triaxial shear strain does not exceed 0.5%. The stiffness degradation curve indicates that significant reduction of the shear stiffness can occur during first two excavations.

REFERENCES

Kolymbas, D. 1991. An outline of hypoplasticity. *Archive of Applied Mechanics* 61:143–151.

PLAXIS. 2010. Material model manual. Technical report, Delft, Netherland.

Masin, D. 2006. Hypoplastic models for fine-grained soils. *PhD thesis, Charles University, Prague*.

Sarabia, F. 2012. Interpretation of the performance of earth retention structures using multi-objective optimization techniques and a hypo-plastic constitutive law. PhD thesis, *Northwestern University, U.S.A*.